Liquid Crystals
Publication details, including instructions for authors and subscription information:
http://www.tandfonline.com/loi/tlct20

Liquid crystal phases generated by supramolecular self-assembly of biforked amphiphilic imidazoles

Oleg N. Kadkin [a], Jigeon Tae [a], So Yeon Kim [a], Eun Ho Kim [a], Eunji Lee [a] & Moon-Gun Choi [a]

[a] Department of Chemistry, BK-21 and Centre for Bioactive Hybrids, Yonsei University, 262 Seongsanno, Seodaemun-Gu, Seoul, 120-749, Korea
Published online: 08 Oct 2009.

To cite this article: Oleg N. Kadkin, Jigeon Tae, So Yeon Kim, Eun Ho Kim, Eunji Lee & Moon-Gun Choi (2009) Liquid crystal phases generated by supramolecular self-assembly of biforked amphiphilic imidazoles, Liquid Crystals, 36:12, 1337-1347, DOI: 10.1080/02678290903225294

To link to this article: http://dx.doi.org/10.1080/02678290903225294

Liquid Crystals,
Vol. 36, No. 12, December 2009, 1337–1347

Taylor & Francis
Taylor & Francis Group

Liquid crystal phases generated by supramolecular self-assembly of biforked amphiphilic imidazoles

Oleg N. Kadkin*, Jigeon Tae, So Yeon Kim, Eun Ho Kim, Eunji Lee and Moon-Gun Choi*

Department of Chemistry, BK-21 and Centre for Bioactive Hybrids, Yonsei University, 262 Seongsanno, Seodaemun-Gu, Seoul 120-749, Korea

(Received 26 June 2009; final form 31 July 2009)

Functional groups with the capability of hydrogen bonding are widely used in the molecular design and preparation of liquid crystalline supramolecular systems, a rapidly growing area of materials showing a high sensitivity towards external stimuli. A series of novel imidazole-containing Schiff's bases replenishing the family of supramolecular liquid crystals has been synthesised and characterised by proton nuclear magnetic resonance, Fourier transform infrared, and ultraviolet–visible spectroscopy, and elemental analyses. Variation of lengths of the terminal alkyl substituents in the obtained amphiphilic imidazoles within 6, 8, 10, 12, 14 and 16 carbon atoms leads to significant changes in their thermal behaviour, micro-segregation and supramolecular self-assembly. Lower homologues were non-mesomorphic, while intermediate members of the homologous series exhibited monotropic bilayered smectic and columnar mesophases. A higher homologue with 16 carbon atoms has an increased trend towards crystallisation of the aliphatic chains and did not exhibit mesomorphism again. The liquid crystalline mesophases were identified and investigated by polarised optical microscopy, differential scanning calorimetry, X-ray diffraction and thermal emission microscopy methods. According to X-ray diffraction characteristics, the smectic mesophase has a bilayered structure where the hydrophilic imidazole groups form a continuous hydrogen bonded network. The interface curvature created by the second alkyl chain leads to the appearance of columnar nanostructures in homologues with 12 and 14 aliphatic carbon atoms.

Keywords: imidazole; liquid crystals; Schiff's base; hydrogen bond; supramolecular assembling; amphiphiles

1. Introduction

Non-covalent interactions play a fundamental role in hierarchical self-assembly and self-organisation of matter including the formation of molecular crystals, liquid crystals, a number of supramolecular nanostructures like colloid micelles, vesicles, tubules, host–guest complexes, and a variety of biological ensembles, such as a DNA double helix, ribosome, lipid bilayers in the cell membranes, etc (*1–6*). In most cases, molecular self-recognition in highly organised supramolecular architectures is implemented by hydrogen bonding. Inducing mesomorphism due to the dimeric structure of carboxylic acids is a well-known example of the action of hydrogen bonds in liquid crystals (*7*). Molecular recognition and complementary self-organisation by means of hydrogen bonds were widely employed for the design and preparation of supramolecular liquid crystalline systems, where a well-defined mesogenic core is formed from different and independent constituents (*8–15*). Another kind of liquid crystalline supramolecular aggregate is realised in both ionic and non-ionic amphiphilic systems by micro-segregation of the lipophilic and hydrophilic parts (*16–23*). Earlier reported polycatenar imidazole-containing mesogens with three alkyl chains in the lipophilic end of the rigid rods showed the hexagonal columnar and cubic mesophases differing from the current biforked imidazoles (*24, 25*). Additionally, hierarchical organisation of disc-like molecules and discoid self-assembled superstructures gives rise to the columnar liquid crystals (*26–29*), which are very promising for applications in microelectronics (*30*). In material sciences, liquid crystals can be used for developing smart molecular systems by exploiting their sensitivity to external magnetic, electric, thermal, optical and chemical stimuli.

The imidazole moiety, which plays an important role in biological systems (*31, 32*), is also well adapted for the formation of hydrogen bonds (*33–37*). Imidazole is a remarkable chemical species derivatives of which have great potential in the area of optical and chemical sensors (*38, 39*), fuel cell membranes (*40–42*), luminescent materials (*43, 44*), ion-conductive electrolytes (*45–47*) and photovoltaic materials for solar cell applications (*48*). There are few works relating to the area of molecular design and synthesis of supramolecular liquid crystalline ensembles on the base of imidazole derivatives (*12, 14, 24–25*). Earlier we demonstrated that linear imidazole-containing Schiff's bases assemble into supramolecular smectogenic bilayers due to the strong intermolecular hydrogen bonding (*49*). In amphiphilic mesogens, the formation

*Corresponding authors. Emails: onk@yonsei.ac.kr; (O. Kadkin); choim@yonsei.ac.kr (M.-G. Choi)

ISSN 0267-8292 print/ISSN 1366-5855 online

DOI: 10.1080/02678290903225294
http://www.informaworld.com

and stabilisation of mesophases are generally achieved by segregation of hydrophilic and hydrophobic parts, and multiple hydrogen bonds provided by, for instance, polyhydroxyl compounds, polyhydroxyamides, or compounds with polyether functions (*20*). Examining a series of biforked imidazole derivatives (see Figure 1) as constituent parts of supramolecular liquid crystals was the main objective of the present studies.

2. Results and discussion

2.1 Syntheses and characterisation

A synthetic route towards imidazole-containing Schiff's bases **3a–f** is illustrated in Scheme 1. The alkoxylated nitrobenzenes **1a–f** were obtained from 4-nitrocatechol by Williamson etherification with corresponding bromoalkanes. Reduction of nitrocompounds **1a–f** was accomplished by hydrogenation in a medium-pressure hydrogenation apparatus in the presence of a Pd/C catalyst (10%). The prepared anilines **2a–f** are rather unstable towards open-air recrystallisation procedures and long storage time. Therefore they were used immediately after isolation from the reaction mixtures in a further condensation procedure with 4(5)-imidazolyl carbaldehyde. As result, Schiff's bases **3a–f** containing 6, 8, 10, 12, 14 and 16 carbon atoms were obtained.

Data of elemental analyses, proton nuclear magnetic resonance (^{1}H NMR), Fourier transform infrared (FT-IR) and ultraviolet–visible (UV-Vis) spectra of the prepared compounds **3a–f** are consistent with the proposed structure. Proton signals of the azomethine group and the imidazole ring are represented in the ^{1}H NMR spectra of **3a–f** by separate singlets in the area of 7.5–8.5 ppm. A proton of the N–H bond does not reveal an ^{1}H NMR signal due to its high mobility connected with the tautomeric equilibrium occurring in the imidazole moiety (*1–6*); see Scheme 2.

However, the N–H bond displays the characteristic valence vibrational band in the FT-IR spectra at ~3170 cm^{-1}, which is red-shifted and broadened because of the hydrogen bonds. The formation of the azomethine CH=N bonds in **3a–f** is reflected by the valence stretching near 1630 cm^{-1}. Benzene and imidazole rings appeared in the area of 1450–1590 cm^{-1}, and the ether C–O–C stretching can be observed in the region of 1220–1260 cm^{-1}. UV-Vis spectra of the compounds **3a–f** are represented by two intensive absorption bands with maxima at about 268 and 338 nm respectively. The first band is associated with π–π^* electron transitions of the aromatic rings, and the second one was assigned to the conjugated azomethine chromophore.

2.2 Thermal properties

Thermal behaviour of a series of imidazole-containing Schiff's bases **3a–f** was investigated by thermal

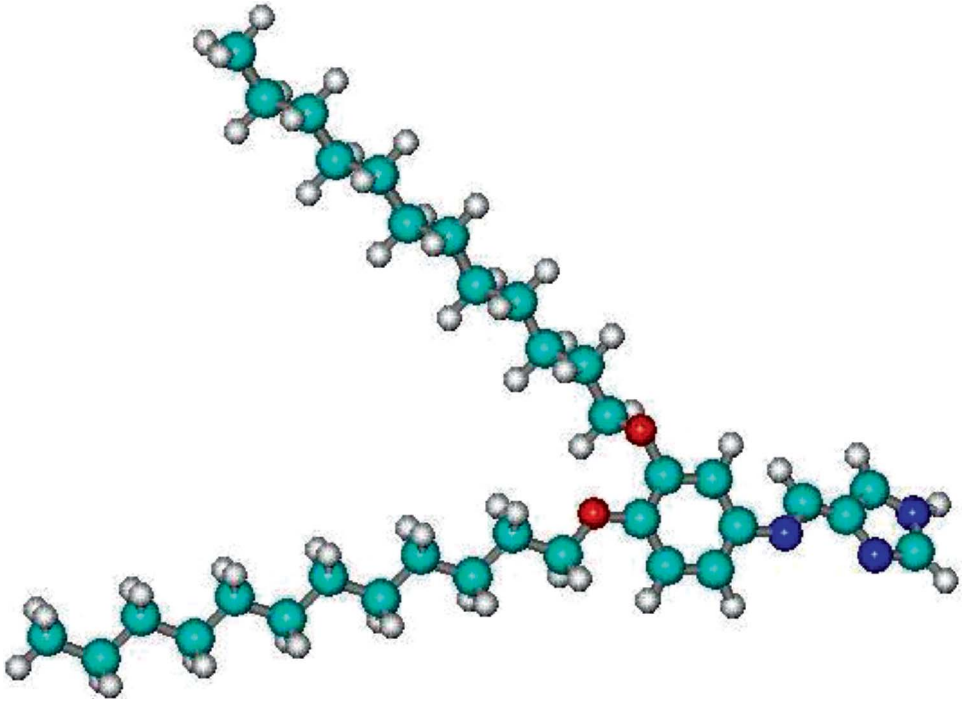

Figure 1. A molecular model of the imidazole-containing amphiphile.

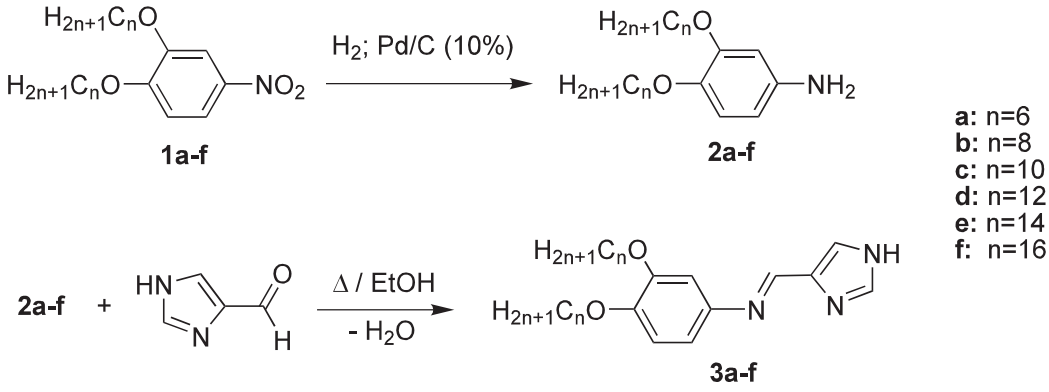

Scheme 1. Synthesis and structure of the imidazole-containing Schiff's bases **3a–f**.

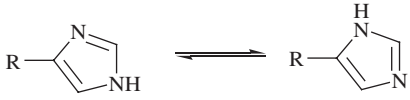

Scheme 2. Tautomeric equilibrium in imidazole derivatives.

polarisation optical microscopy (POM) and differential scanning calorimetry (DSC) (Table 1). The homologues **3a,b** with hexyloxy and octyloxy terminal alkyl chains did not exhibit mesomorphism. Monotropic, i.e. thermodynamically metastable, mesophases were observed in a case of compounds **3c–e** with n = 10, 12 and 14. Slow kinetics of crystallisation leads to partial vitrification of the samples, as could be seen from the sums of heat effects in the cooling course of DSC. The latter values were as rule lower than for the heating course in typical experiments with a scanning rate 5°C/min. This conforms to the well-known fact that monotropic mesophases are normally observed when the thermodynamically more stable crystal phase is bypassed because of slow kinetics of recrystallisation.

DSC traces and an optical microphotograph of compound **3c** with n = 10 are represented in Figure 2. Although the mesophase of **3c** was not detected by the DSC method, a thread-like texture, presumably of the lamellar mesophase, was observed under a polarising light microscope. Though a crystallisation peak in DSC experiments was observed in the area of 40°C at the scanning rate of 5°C/min, annealing of the sample in the region of 55–60°C normally leads to the appearance of crystal spherulites in the background of the smectic mesophase.

Two kinds of mesophases were detected in compound **3d** with n = 12 by both DSC and POM methods. The first mesophase after the isotropic liquid state was identified as a lamellar mesophase (see Figure 3). It forms a sand-like texture upon cooling from the isotropic liquid. The lamellar structure of this mesophase also was confirmed by the X-ray diffraction (XRD) method. A scattering peak corresponding to an interlayer spacing distance of 3.82 nm in the small angle region and a broad reflection centred near 0.44 nm were observed in XRD diagrams (Figure 4). A dimension of the single molecule of **3d** in the longest direction

Table 1. Types of phase transitions, temperatures and corresponding enthalpies obtained by polarising optical microscopy and differential scanning calorimetry methods for compounds **3a–f.**

	Phase transitions, °C (ΔH, kJ × mol^{-1})[a]	
Compound	Heating course	Cooling course
3a	Cr 70.9(15.2) I	I 30.0 Cr
3b	Cr 73.8(14.2) I	I 50.0 Cr
3c	Cr 81.5(56.6) I	I 61.6[b] Sm 35.l(–37.6) Cr
3d	Cr 90.0(40.6) I	I 71.4(–4.1) Sm 43.1(–2.0) Col_x 34.9(–27.8) Cr
3e	Cr 95.5(51.3) I	I 70.0 Sm 57.5(–22.3) Col_x 43.5(–6.8) Cr
3f	Cr_1 58.7(7.51) Cr_2 94.1(51.4) I	I 48.6(–51.2) Cr

[a] Cr, crystal; I, isotropic liquid; Sm, smectic; Col_x, columnar mesophases.
[b] The related temperature was detected only by polarising optical microscopy, a differential scanning calorimetry peak is not resolved.

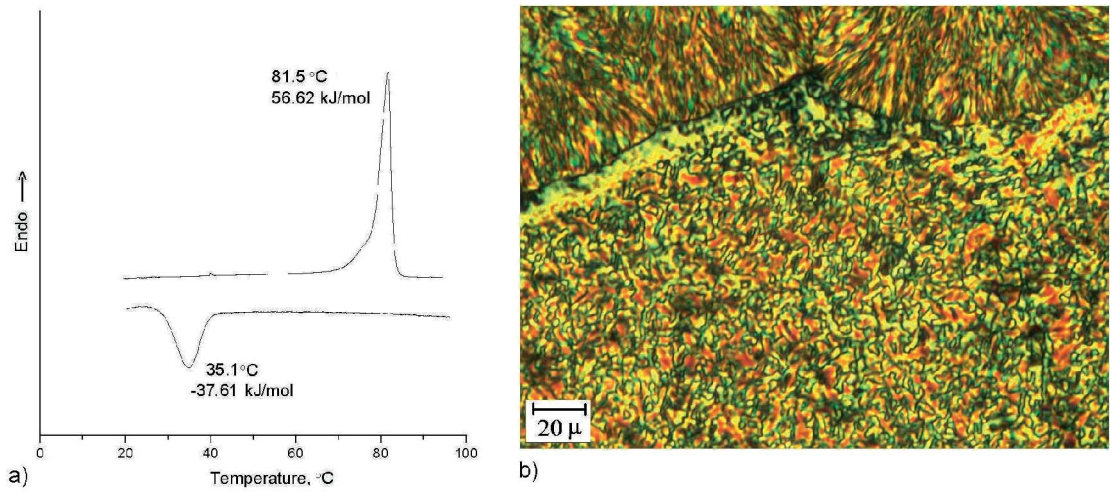

Figure 2. (a) Differential scanning calorimetry traces of compound **3c** at scanning rate 5°C/min (the upper curve is a heating course, and the lower curve is a cooling course); (b) a photomicrograph of a schlieren texture of the smectic mesophase taken at 55°C with a crystallisation area in the upper part.

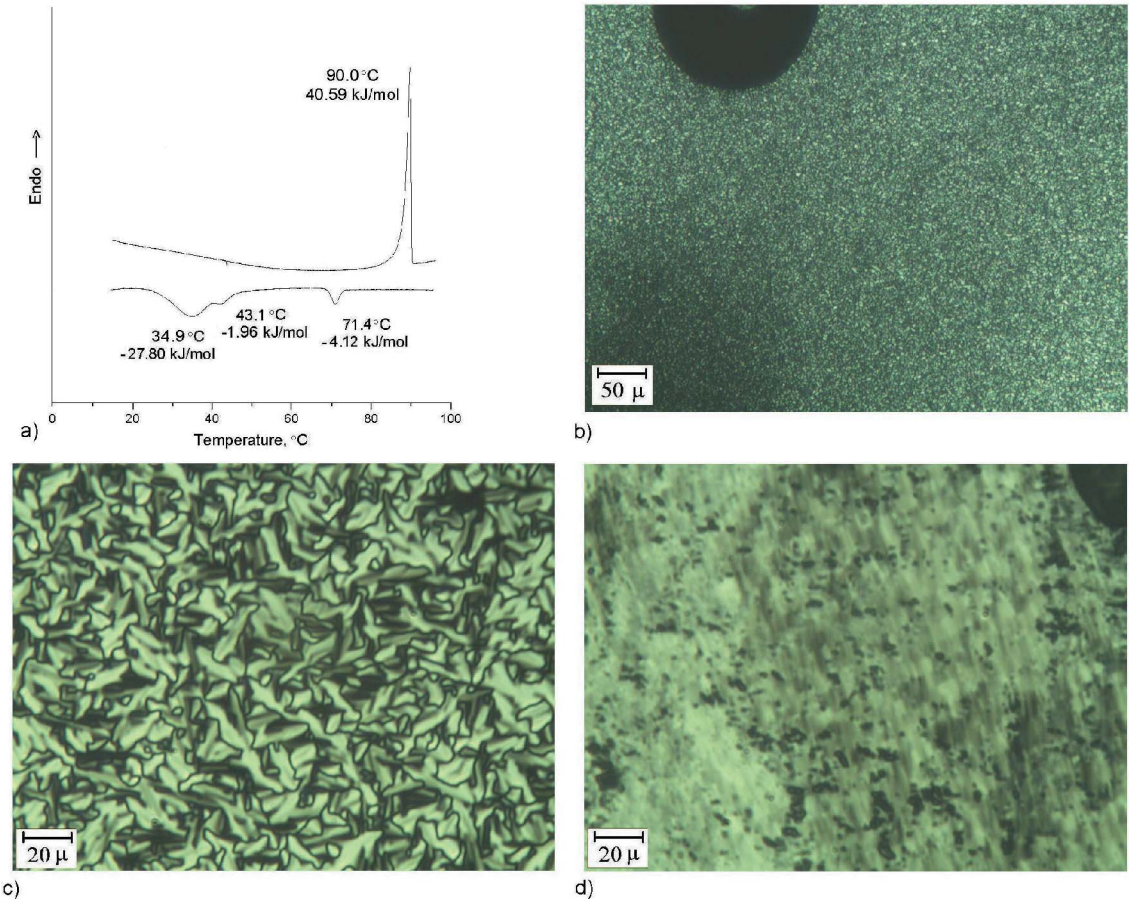

Figure 3. (a) Differential scanning calorimetry traces of compound **3d** at scanning rate 5°C/min; (b) a sand-like texture of the smectic mesophase at 70°C; (c) a dendritic comb-like texture of the columnar mesophase at 43°C; (d) the previous sample after the sheared deformation.

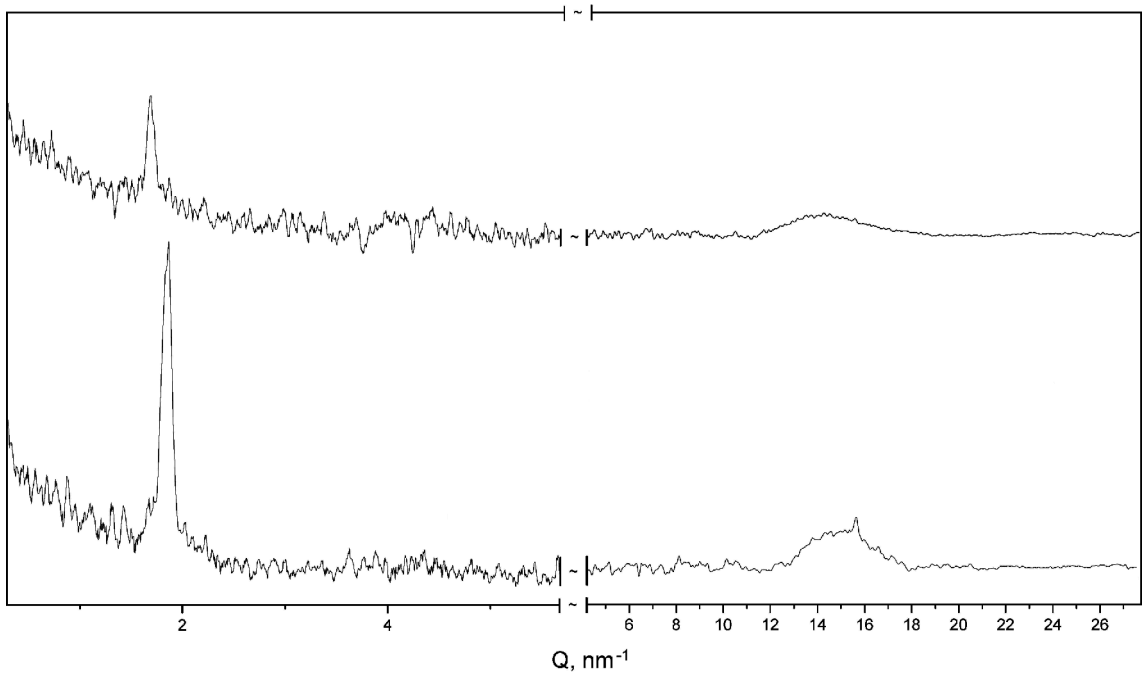

Figure 4. X-ray scattering diagrams of **3d** obtained at 71°C (the upper graph) and 60°C (the lower graph) on the sample gradually cooled from the isotropic state.

was found as 2.6 nm by computer modelling, which is far below the experimental interlayer spacing. This suggests that intermolecular hydrogen bonds lead to the head-to-head bilayered supramolecular organisation (Figure 5). Simulation of the smectic C bilayers by using the computer molecular models gave a satisfactory correlation with the experimental interlayer spacing distance. In general, a peak related to the lamellar structure is weakly articulated in the XRD diagram, so that means the smectic layers are highly disordered.

Upon further cooling a transient optically isotropic pattern and then growth of a dendritic-like texture were

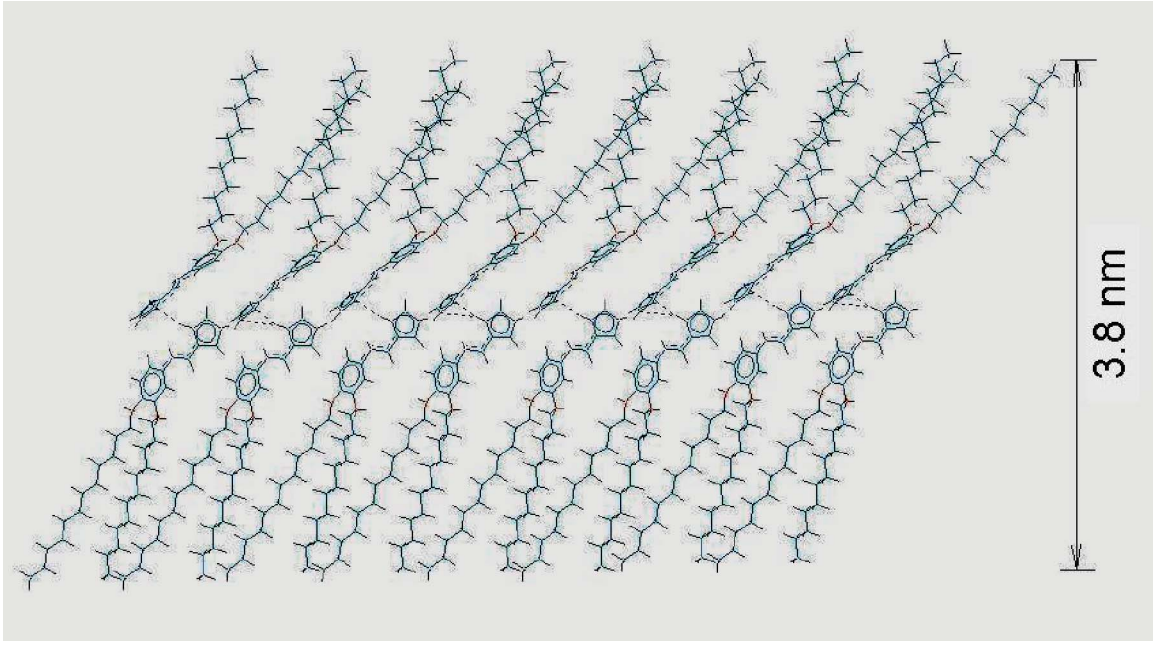

Figure 5. Computer simulation of the smectic C bilayers in **3d**.

observed under POM. The latter texture can be sheared between microscope slides (Figure 3(d)). In view of low fluidity we have assigned it to the columnar mesophase. The origin of a non-birefringent dark texture is not completely clear; it might be connected with a transitory state during the development of columnar aggregates from the lamellar mesophase. Further cooling leads to appearance of spherulitic crystals. Significant change of an interlayer spacing distance from 3.82 nm to a much shorter interlayer spacing of 3.38 nm was observed in XRD of the columnar mesophase, which could be connected with the formation of columnar aggregates from the initial lamellar state. Owing to low intensity of X-ray scattering peaks, the reflections other than 110 are not resolved in the small angle region. In the wide angle region, a broad correlation of terminal alkyl chains and a small reflection at 0.41 nm, which is presumably corresponding to the stacking distance within the columns, can be identified (Figure 4).

Compound **3e** with tetradecyloxy substituents exhibited the smectic and columnar mesophases upon cooling of the specimen from the isotropic liquid state. A broad transition to the columnar mesophase was detected by DSC (Figure 6). Although an isotropic liquid-to-smectic transition is embedded in the broad peak of the columnar phase transition, the smectic mesophase was observed by POM and XRD (Figures 6(b) and 7). In all probability a schlieren texture exhibited by the smectic mesophase of the biforked mesogenic imidazoles is a consequence of the hydrogen-bonded bilayered structure where the central rigid rods are tilted in relation to the smectic planes. A schlieren texture transforms to a homogeneous coloured pattern upon shearing of the microscope slides (Figure 6(c)). Further cooling leads to a significant transformation of the POM texture, seemingly connected with the appearance of columnar arrangement (Figure 6(d)). An optical texture similar to that of Figure 3(c) was also observed. The sample crystallises into spherulitic formations below 40°C.

The thermodynamic instability of the observed mesophases makes it difficult to obtain their XRD characteristics. However, a typical pattern of the bilayered smectic mesophase of **3e** was afforded in

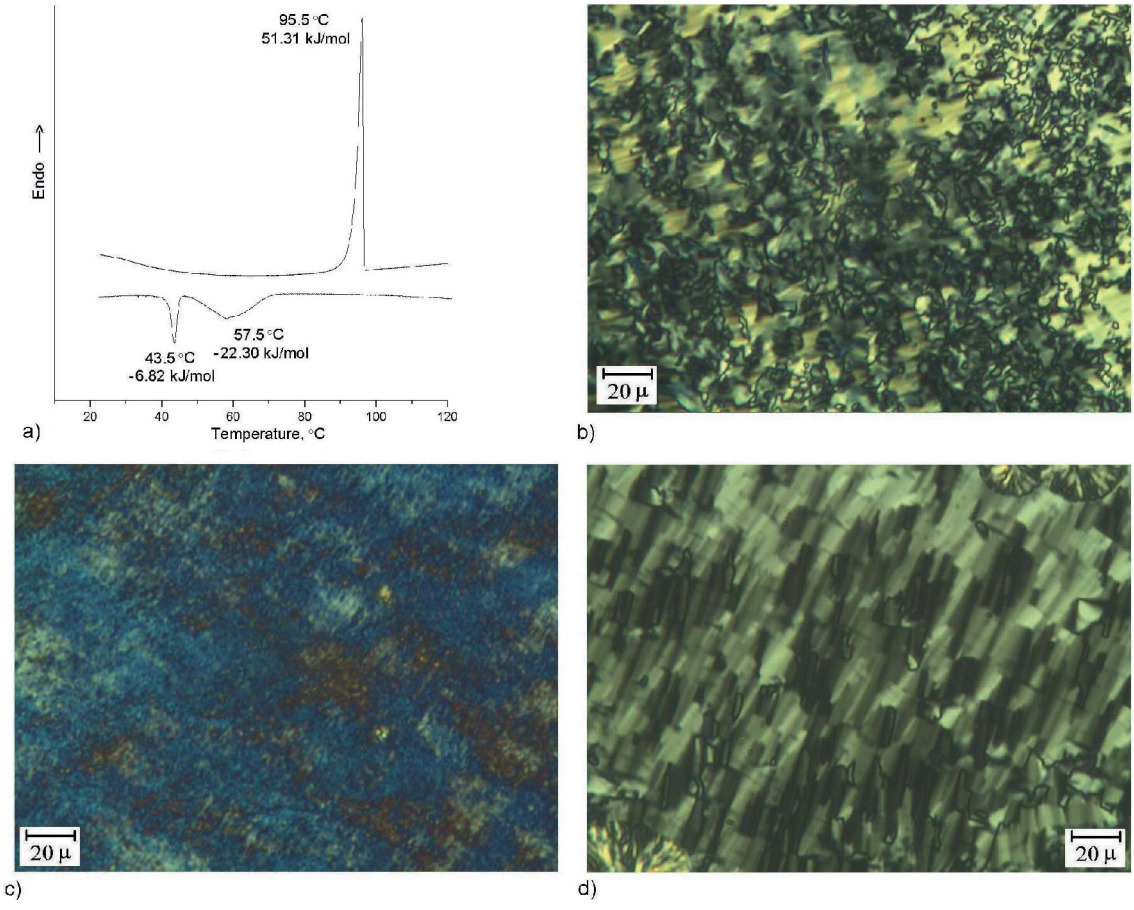

Figure 6. (a) Differential scanning calorimetry traces of compound **3e** at scanning rate 5°C/min; (b) a schlieren texture of the smectic mesophase at 69°C; (c) the previous sample after shearing; (d) a broken focal-conic texture of the columnar mesophase at 62°C.

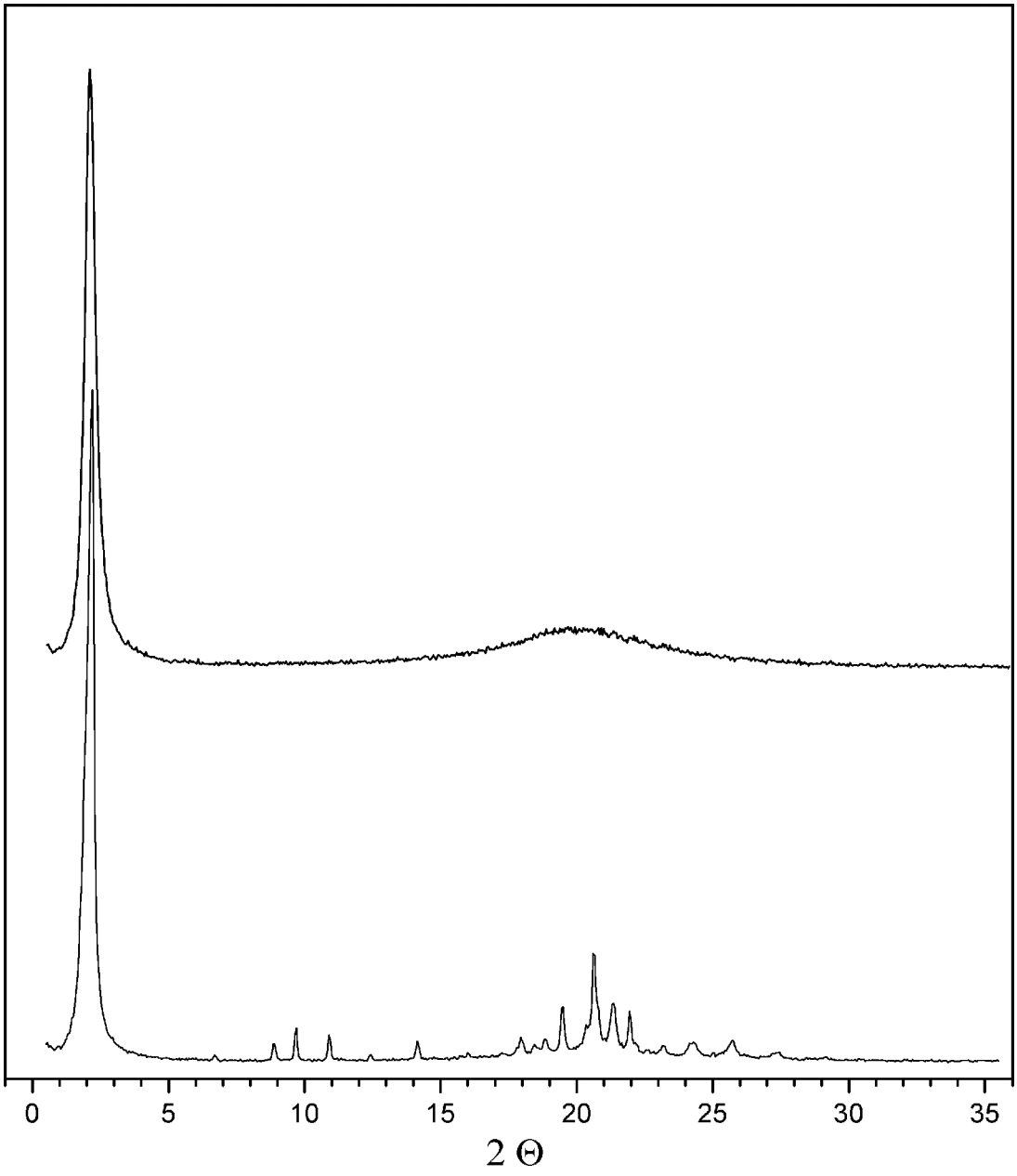

Figure 7. X- ray diffraction diagrams of compound **3e** at 70°C (the upper graph) and 65°C (the lower graph) on the sample gradually cooled from the isotropic state.

X-ray scattering experiments (Figure 7). Accordingly, an interlayer spacing of 4.20 nm was found between the smectic lamellas, which points at their bilayered structure. A difference between interlayer spacing distances of **3d** and **3e** is 0.38 nm, and this complies well with the addition on average of four chemical bond increments into the bilayers. In a condition of XRD experiments **3e** crystallised at 65°C as a number of peaks appeared in the wide-angle region. Impact cooling of the columnar mesophase state of **3e** was carried out, and then the sample was cryo-sectioned for the thermal emission microscopy (TEM) experiments. One can see on the TEM images (Figure 8) elongated aggregates corresponding to a side view on the columns. In some spots round dots can be observed, which correspond to a view of the columns from the top. An approximate diameter of the columns can be estimated as ~4 nm from the TEM patterns.

The last member of the homologous series **3f** with $n = 16$ did not exhibit mesomorphism upon cooling

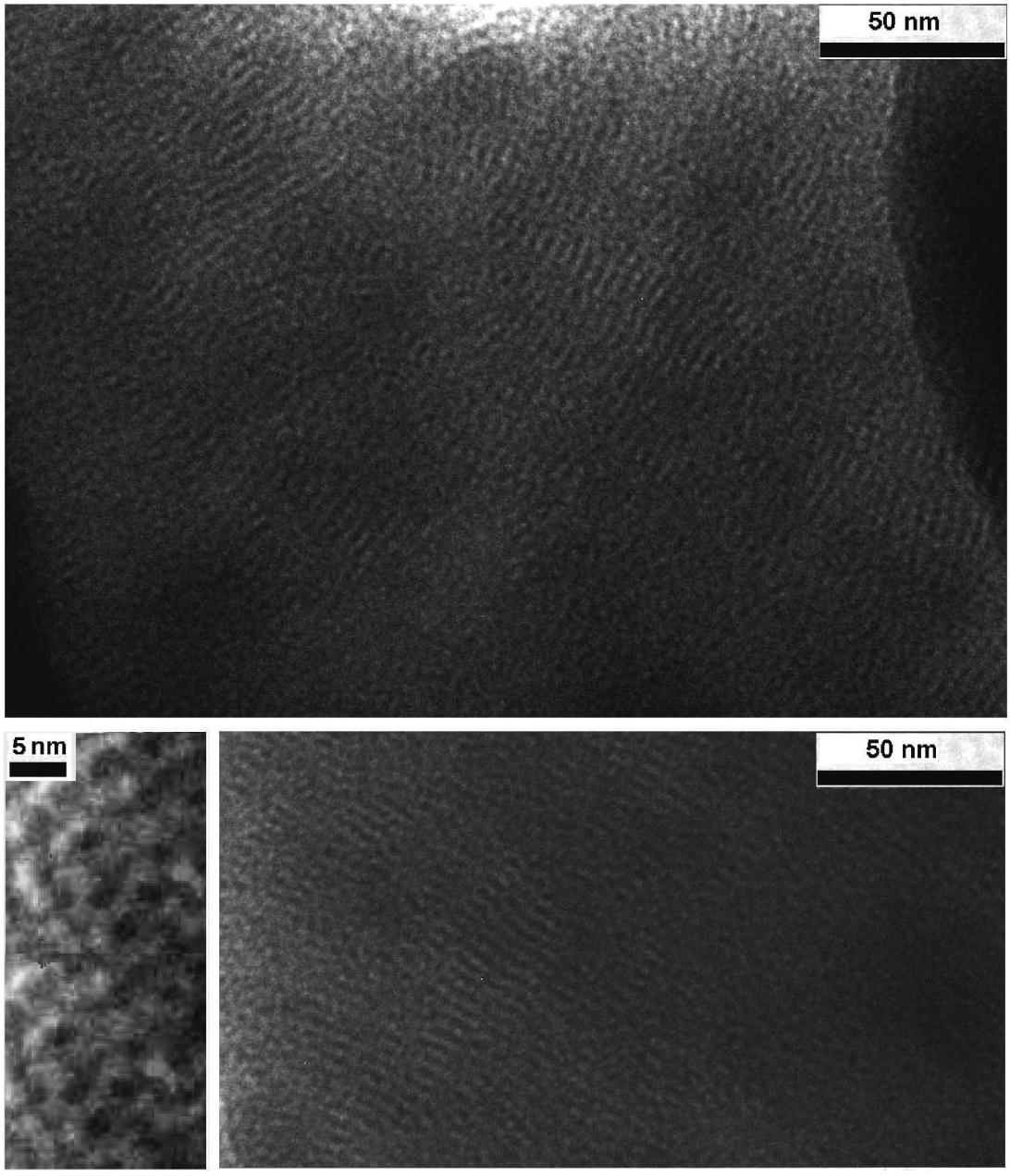

Figure 8. Thermal emission microscopy images of compound **3e**: the upper picture is a side view on the columns; the lower left picture is a magnified area with round spots derived from a top view on the columns; the lower right picture is a mixed area with both dotted and striped textures.

from the isotropic melt, but rather displayed spherulitic formations which are typical for supramolecular crystal agglomerates.

3. Experimental details

3.1 General details

The 3,4-dialkyloxynitrobenzenes **1** and corresponding 3,4-dialkyloxyanilines **2** were synthesised by using procedures from the literature (*50*). Reagent-grade chemicals and solvents were purchased from Aldrich (Yongin, Kyounggi-Do, Korea, Korea Branch). Solvents were dried and freshly distilled just before use. ^{1}H NMR spectra were measured on a Bruker AM 400 with internal TMS standard. FT-IR spectra were performed on Nicolet Abatar-360 FT-IR spectrometer. UV and visible spectra in the region of 200–800 nm were recorded on a spectrophotometer Shimadzu UV-1650PC. Elemental analyses were

performed on a Fisons instrument 2A1108 at Korea Institute of Science and Technology. DSC thermographs were obtained on Perkin Elmer Diamond DSC with a scan rate of 2°C/min. Thermo-optical observations were carried out on a Nikon Eclipse E600 Pol optical polarised microscope equipped with a Mettler Toledo FP82 HT hot stage system and Mettler FP90 central processor. Microphotographs were obtained with a Moticam 2300 digital camera. X-ray scattering measurements of the compound **3d** were conducted on an apparatus consisting of an 18-kW rotating anode X-ray generator system (Rigaku Co.) operated at 46 kV × 20 mA, and mirror optics with point focusing. Copper Kα radiation (=1.5418 Å) from a 0.1 mm × 1 mm microfocus cathode was used. Two-dimensional (2-D) diffraction patterns were recorded on imaging plates. The distance between sample and imaging plate was 68 cm for small-angle scattering, 18 cm for wide-angle scattering. The sample was held in an aluminium sample holder, which was sealed with the window of 7 μm-thick Kapton films on both sides. The sample was heated with two cartridge heaters and the temperature of the samples was monitored by a thermocouple placed close to the sample. X-ray scattering measurements for **3e** were performed in transmission mode with synchrotron radiation at the 10C1 X-ray beam line at the Pohang Accelerator Laboratory, Pohang, South Korea. A wavelength of the X-ray radiation beam was 1.5401 Å. Molecular models and mesophase packing simulations were performed using the program Hyperchem 7, from Hypercube, Inc. (Gainesville, Florida, USA). TEM images were obtained at 120 keV using a JEOL 2010 hi-resolution transmission electron microscope (JEOL Ltd., Tokyo, Japan). Ultrathin sectioning of the specimen was performed in cryogenic conditions at –40°C using an ultramicrotome RMC Powertome-XL with a glass knife (Tucson, Arizona, USA). Thin sections of the specimen were transferred onto a carbon-coated copper grid and stained with RuO_4 vapour.

3.2 (E)-N-(1H-imidazole-4(5)-yl)methylene-(3,4-dihexyloxy)aniline (3a)

3,4-dihexyloxyaniline **2a** (0.50 g, 1.71 mmol) and 1*H*-imidazole-4(5)-carbaldehyde (0.16 g, 1.71 mmol) were dissolved separately in a minimal amount of hot ethanol. Two solutions were combined and refluxed for 2 hours in the presence of 1–2 drops of acetic acid. A cream-coloured precipitate was formed upon cooling to –20°C. The product was filtered off and recrystallised from ethanol upon cooling to –20°C. Yield 0.52 g (72%). ^{1}H NMR ($CDCl_3$): δ = 0.91 (t, 6H, CH_3, $J_{H,H}$ = 7.5 Hz), 1.20–1.50 (m, 12H, CH_2), 1.82 (m, 4H, $OCH_2C\underline{H}_2$), 4.02 (m, 4H, OCH_2), 6.70–7.00 (m, 3H, C_6H_3), 7.54 (s, 1H, CH-imidaz), 7.75 (s, 1H, CH-imidaz); 8.39 (s, 1H, CH-azometh). FT-IR (KBr, cm^{-1}): $\tilde{\nu}$ = 3170 (br, N-H), 2964, 2931, 2868, 2854, 1626 (C=N), 1591, 1508, 1469, 1456, 1256, 1227, 1134, 858. UV-vis (CH_2Cl_2, nm): λ = 268 and 338; log ε ($dm^3 \times mol^{-1} \times cm^{-1}$) = 4.17 and 4.12. Elemental analysis calculated for $C_{22}H_{33}N_3O_2$: C 71.12%, H 8.95%, N 11.31%. Found: C 70.64%, H 8.89%, N 10.97%.

3.3 (E)-N-(1H-imidazole-4(5)-yl)methylene-(3,4-dioctyloxy)aniline (3b)

The compound was prepared as described above for **3a** from 3,4-dioctyloxyaniline **2b** (0.50 g, 1.43 mmol) and 1*H*-imidazole-4(5)-carbaldehyde (0.14 g, 1.43 mmol). Yield 0.50 g (78%). ^{1}H NMR ($CDCl_3$): δ = 0.89 (t, 6H, CH_3, $J_{H,H}$ = 7.5 Hz), 1.20–1.50 (m, 20H, CH_2), 1.82 (m, 4H, $OCH_2C\underline{H}_2$), 4.02 (m, 4H, OCH_2), 6.70–7.00 (m, 3H, C_6H_3,), 7.54 (s, 1H, CH–imidaz), 7.75 (s, 1H, CH-imidaz), 8.39 (s, 1H, CH-azometh). FT-IR (KBr, cm^{-1}): $\tilde{\nu}$ = 3173 (br, N-H), 2953, 2926, 2854, 1634 (C=N), 1586, 1510, 1467, 1449, 1261, 1231, 1127, 856. UV-vis (CH_2Cl_2, nm): λ = 264 and 339; log ε ($dm^3 \times mol^{-1} \times cm^{-1}$) = 4.05 and 3.90. Elemental analysis calculated for $C_{26}H_{41}N_3O_2$: C 73.03%, H 9.66%, N 9.83%. Found: C 72.50%, H 9.59%, N 9.47%.

3.4 (E)-N-(1H-imidazole-4(5)-yl)methylene-(3,4-didecyloxy)aniline (3c)

The compound was prepared as described above for **3a** from 3,4-didecyloxyaniline **2c** (0.50 g, 1.23 mmol) and 1H-imidazole-4(5)-carbaldehyde (0.12 g, 1.23 mmol). Crystallisation was performed at room temperature. Yield 0.54 g (91%). ^{1}H NMR ($CDCl_3$): δ = 0.88 (t, 6H, CH_3, $J_{H,H}$ = 7.5 Hz), 1.20–1.50 (m, 28H, CH_2), 1.82 (m, 4H, $OCH_2C\underline{H}_2$), 4.02 (m, 4H, OCH_2), 6.70–7.00 (m, 3H, C_6H_4,), 7.54 (s, 1H, CH-imidaz), 7.71 (s, 1H, CH-imidaz), 8.40 (s, 1H, CH-azometh). FT-IR (KBr, cm^{-1}): $\tilde{\nu}$ = 3173 (br, N-H), 2954, 2922, 2850, 1630 (C=N), 1593, 1513, 1467, 1265, 1229, 1132, 838. UV-vis (CH_2Cl_2, nm): λ = 268 and 337; log ε ($dm^3 \times mol^{-1} \times cm^{-1}$) = 3.97 and 3.95. Elemental analysis calculated for $C_{30}H_{49}N_3O_2$: C 74.49%, H 10.21%, N 8.69%. Found: C 74.56%, H 10.23%, N 8.75%.

3.5 (E)-N-(1H-imidazole-4(5)-yl)methylene-(3,4-didodecyloxy)aniline (3d)

The compound was prepared as described above from 3,4-bis(dodecyloxy)aniline **2d** (0.50 g, 1.08 mmol) and 1*H*-imidazole-4(5)-carbaldehyde (0.10 g, 1.08 mmol). Yield 0.52 g (91%). ^{1}H NMR ($CDCl_3$): δ = 0.85 (t, 6H,

CH_3, $J_{H,H}$ = 7.5 Hz), 1.20–1.50 (m, 36H, CH_2), 1.80 (m, 4H, $OCH_2C\underline{H}_2$), 4.02 (m, 4H, OCH_2), 6.70–7.00 (m, 3H, C_6H_4,), 7.54 (s, 1H, CH-imidaz), 7.71 (s, 1H, CH-imidaz), 8.40 (s, 1H, CH-azometh). FT-IR (KBr, cm^{-1}): $\tilde{\nu}$ = 3172 (br, N-H), 2920, 2851, 1630 (C=N), 1593, 1514, 1467, 1265, 1229, 1131, 844. UV-vis (CH_2Cl_2, nm): λ = 268 and 338; log ε ($dm^3 \times mol^{-1} \times cm^{-1}$) = 4.06 and 4.04. Elemental analysis calculated for $C_{34}H_{57}N_3O_2$: C 75.65%, H 10.64%, N 7.78%. Found: C 75.67%, H 10.58%, N 7.89%.

3.6 (E)-N-(1H-imidazole-4(5)-yl)methylene-(3,4-ditetradecyloxy)aniline (3e)

The compound was prepared as described above from 3,4-bis(tetradecyloxy)aniline **2e** (0.50 g, 0.97 mmol) and 1*H*-imidazole-4(5)-carbaldehyde (0.09 g, 0.97 mmol). Yield 0.53 g (91%). ^{1}H NMR ($CDCl_3$): δ = 0.88 (t, 6H, CH_3, $J_{H,H}$ = 7.5 Hz), 1.20–1.50 (m, 44H, CH_2), 1.80 (q, 4H, $OCH_2C\underline{H}_2$), 4.02 (q, 4H, OCH_2), 6.70–7.00 (m, 3H, C_6H_4,), 7.55 (s, 1H, CH-imidaz), 7.76 (s, 1H, CH-imidaz), 8.39 (s, 1H, CH-azometh). FT-IR (KBr, cm^{-1}): $\tilde{\nu}$ = 3178 (br, N-H), 2919, 2850, 1630 (C=N), 1593, 1513, 1467, 1265, 1230, 1132, 846. UV-vis (CH_2Cl_2, nm): λ = 269 and 337; log ε ($dm^3 \times mol^{-1} \times cm^{-1}$) = 4.17 and 4.14. Elemental analysis calculated for $C_{38}H_{65}N_3O_2$: C 76.59%, H 10.99%, N 7.05%. Found: C 76.26%, H 10.77%, N 7.28%.

3.7 (E)-N-(1H-imidazole-4(5)-yl)methylene-(3,4-dihexadecyloxy)aniline (3f)

The compound was prepared as described above from 3,4-bis(hexadecyloxy)aniline **2f** (0.50 g, 0.87 mmol) and 1*H*-imidazole-4(5)-carbaldehyde (0.08 g, 0.87 mmol). The yield was 0.54 g (94%). ^{1}H NMR ($CDCl_3$): δ = 0.88 (t, 6H, CH_3, $J_{H,H}$ = 7.5 Hz), 1.20–1.50 (m, 52H, CH_2), 1.82 (m, 4H, $OCH_2C\underline{H}_2$), 4.02 (m, 4H, OCH_2), 6.70–7.00 (m, 3H, C_6H_4,), 7.53 (s, 1H, CH-imidaz), 7.74 (s, 1H, CH-imidaz), 8.40 (s, 1H, CH-azometh). FT-IR (KBr, cm^{-1}): $\tilde{\nu}$ = 3178 (br, N-H), 2920, 2849, 1629 (C=N), 1592, 1511, 1468, 1264, 1229, 1127, 849. UV-vis (CH_2Cl_2, nm): λ = 267 and 337; log ε ($dm^3 \times mol^{-1} \times cm^{-1}$) = 4.08 and 4.01. Elemental analysis calculated for $C_{42}H_{73}N_3O_2$: C 77.36%, H 11.28%, N 6.44%. Found: C 77.48%, H 11.47%, N 5.94%.

4. Conclusions

Novel representatives of the family of amphiphilic supramolecular mesogens on the base of imidazole derivatives have been synthesised and characterised by ^{1}H NMR, FT-IR, UV-vis and elemental analyses. It has been demonstrated that the thermal behaviour, micro-segregation and supramolecular self-assembly of the synthesised amphiphiles are highly sensitive to their hydrophilic–lipophilic balance. A variation of the lengths of the terminal alkyl substituents within 6, 8, 10, 12, 14 and 16 carbon atoms results in non-mesomorphic behaviour of the lower and higher homologues, and lamellar and columnar mesomorphism in a case of intermediate lengths of the terminal alkyl chains. The monotropic smectic and columnar mesophases were identified by POM and DSC methods for the compounds with 10, 12 and 14 carbon atoms in the aliphatic tails. In the same conditions anticipated crystallisation of the aliphatic parts prevents the formation of the mesophases in the higher homologue with 16 carbon atoms in the terminal substituents. Thermooptical studies, XRD measurements and molecular modelling of the synthesised compounds suggest a bilayered structure with a continuous network of hydrogen bonds in the smectic mesophases. The columnar arrangement was additionally confirmed by TEM imaging of the supercooled samples.

Acknowledgements

This work has been supported by a grant from the Korea Science and Engineering Foundation (KOSEF) through the Center for Bioactive Molecular Hybrids (CBMH), and the program Brain Korea 21 (BK-21). Pohang Accelerator Laboratory is acknowledged for providing X-ray beam from their synchrotron facilities.

References

(1) de Gennes, P.G.; Prost, J. *The Physics of Liquid Crystals*; 2nd edition, Oxford University Press: New York, 1993.
(2) Gray, G.W.; Vill, V.; Spiess H.W.; Demus, D.; Goodby, J.W. *Physical Properties of Liquid Crystals*; Wiley-VCH: New York, 1999.
(3) Chandrasekhar, S. *Liquid Crystals*; 2nd edition, Cambridge University Press: Cambridge, 1992.
(4) Collings, P.J. *Liquid Crystals: Nature's Delicate Phase of Matter*; 2nd edition, Princeton University Press: Princeton, NJ, 1990.
(5) Lehn, J.-M. *Supramolecular Chemistry*; VCH: New York, 1995.
(6) Brown, G.H.; Wolken, J.J. *Liquid Crystals and Biological Structures*; Academic Press: New York, 1979.
(7) Bennett, G.M.; Jones, B. *J. Chem. Soc.* **1939**, 420–425.
(8) Kato, T.; Frechet, J.M.J. *J. Am. Chem. Soc.* **1989**, *111*, 8533–8534.
(9) Brienne, M.-J.; Gabard, J.; Lehn, J.-M.; Stibor, I. *J. Chem. Soc., Chem. Commun*. **1989**, 1868–1870.
(10) Paleos, C.M.; Tsiourvas, D. *Angew. Chem. Int. Ed. Engl.* **1995**, *34*, 1696–1711.
(11) Kato, T. In *Handbook of Liquid Crystals*; Demus, D.; Goodby; J.W.; Gray, G. W.; Spiess, H.-W.; Vill, V., Eds.; Wiley-VCH: Weinheim, Germany, 1998; Vol. 2B, Chapter XVII, pp. 969–978.

(12) Kato, T.; Kawakami, T. *Chem. Lett.* **1997**, 211–212.
(13) Deschenaux, R.; Monnet, F.; Serrano, E.; Turpin, F.; Levelut, A.-M. *Helv. Chim. Acta*, **1998**, *81*, 2072–2077.
(14) Kraft, A.; Reichert, A.; Kleppinger, R. *Chem. Commun.* **2000**, 1015–1016.
(15) Massiot, P.; Impéror-Clerc, M.; Veber, M.; Deschenaux, R. *Chem. Mater.* **2005**, *17*, 1946–1951.
(16) Skoulios, A.; Guillon, D. *Mol. Cryst. Liq. Crvst.* **1988**, *165*, 317–332.
(17) Paleos, C.M. *Mol. Cryst. Liq. Crvst.* **1994**, *243*, 159–183.
(18) Surez, M.; Lehn, J.-M.; Zimmerman, S.C.; Skoulios, A.; Heinrich, B. *J. Am. Chem. Soc.* **1998**, *120*, 9526–9532.
(19) Tschierske, C. *J. Mater. Chem.* **1998**, *8*, 1485–1508.
(20) Borisch, K.; Diele, S.; Göring, P.; Kresse, H.; Tschierske, C. *J. Mater. Chem.* **1998**, *8*, 529–543.
(21) Kato, T.; *Science*, **2002**, *295*, 2414–2418.
(22) Kato, T.; Mizoshita, N. *Curr. Opin. Sol. St. Mater. Sci.* **2002**, *6*, 579–587.
(23) Abeygunaratne, S.; Chien, L.-C.; Vill, V. *Liq. Cryst.* **2007**, *34*, 441–445.
(24) Seo, S.H.; Park, J.H.; Tew, G.N.; Chang, J.Y. *Soft Matter*, **2006**, *2*, 886–891.
(25) Seo, S.H.; Tew, G.N.; Chang, J.Y. *Tetrahedr. Lett.* **2007**, *48*, 6839–6844.
(26) Kumar, S. *Chem. Soc. Rev.* **2006**, *35*, 83–109.
(27) Chandrasekhar, S. In *Handbook of Liquid Crystals*; Demus, D.; Goodby; J.W.; Gray, G.W.; Spiess, H.-W.; Vill, V., Eds.; Wiley-VCH: Weinheim, 1998; Vol. 2B, Chapter VIII, pp. 749–780.
(28) Chandrasekhar, S.; Ranganathart, G.S. *Rep. Prog. Phys.* **1990**, *53*, 57–84.
(29) Laschat, S.; Baro, A.; Steinke, N.; Giesselmann, F. *Angew. Chem. Int. Ed.* **2007**, *46*, 4832–4887.
(30) Sergeyev, S.; Pisula, W.; Geerts.;Y.H. *Chem. Soc. Rev.* **2007**, *36*, 1902–1929.
(31) Brown, E.G. *Ring Nitrogen and Key Biomolecules*; Kluwer Academic: Dordrecht, 1998.
(32) Pozharskii, A.F.; Soldatenkov, A.T.; Katritzky, A.R. *Heterocycles in Life and Society*; John Wiley & Sons: Chichester, 1997.
(33) Amini, S.K.; Hadipour, N.L.; Elmi, F. *Chem. Phys. Lett.* **2004**, *391*, 95–100.
(34) Ueda, T.; Nagatomo, S.; Masui, H.; Nakamura, N. *Z. Naturforsch.* **1999**, *54a*, 437–442.
(35) Wei, Y.; Dios, A.C.D.; McDermott, A.E. *J. Am. Chem. Soc.* **1999**, *121*, 10389–10394.
(36) Nagatomo, S.; Takeda, S.; Tamura, H.; Nakamura, N. *Bull. Chem. Soc. Jpn.* **1995**, *68*, 2783–2789.
(37) Torrent, M.; Musaev, D.G.; Morokuma, K.; Ke, S.-C.; Warncke, K. *J. Phys. Chem. B*, **1999**, *103*, 8618–8627.
(38) Fukuda, N.; Kim, J.Y.; Fukuda, T.; Ushijima, H.; Tomada K. *Jpn. J. Appl. Phys.* **2006**, *45*, 460–464.
(39) Chao, H.; Ye, B.-H.; Zhang, Q.-L.; Ji, L.-N. *Inorg. Chem. Commun.* **1999**, *2*, 338–340.
(40) Schuster, M.; Meyer, W.H.; Wegner, G.; Herz, H.G.; Ise, M.; Schuster, M.; Kreuer, K.D.; Maier J. *Solid State Ionics* **2001**, *145*, 85–92.
(41) Münch, W.; Kreuer, K.-D.; Silvestri, W.; Maier, J.; Seifert, G. *Solid State Ionics* **2001**, *145*, 437–443.
(42) Pu, H.; Qiao, L. *Macromol. Chem. Phys*. **2005**, *206*, 263–267.
(43) Knölker, H.-J.; Hitzemann, R.; Boese, R. *Chem. Ber.* **1990**, *123*, 327–339.
(44) Zhao, L.; Li, S.B.; Wen, G.A.; Peng, B.; Huang, W. *Mater. Chem. Phys.* **2006**, *100*, 460–463.
(45) Yoshio, M.; Kagata, T.; Hoshino, K.; Mukai, T.; Ohno, H.; Kato, T. *J. Amer. Chem. Soc.* **2006**, *128*, 5570–5577.
(46) Kishimoto, K.; Suzawa, T.; Yokota, T.; Mukai, T.; Ohno, H.; Kato, T. *J. Amer. Chem. Soc.* **2005**, *127*, 15618–15623.
(47) Yoshio, M.; Mukai, T.; Ohno, H.; Kato, T. *J. Amer. Chem. Soc.* **2004**, *126*, 994–995.
(48) Wang, M.; Xiao, X.; Zhou, X.; Li, X.; Lin, Y. *Sol. Energy Mater. Sol. Cells*, **2007**, *91*, 785–790.
(49) Kadkin, O.N.; Tae, J.; Kim, E.H.; Kim, S.Y.; Choi, M.-G. *Supramol. Chem.* **2009**, DOI: 10.1080/10610270802709386.
(50) Yoo, Y-S; Im, J.-H.; Han, B.-H.; Lee, M.; Choi, M.-G. *Bull. Kor. Chem. Soc.* **2001**, *22*, 1350.